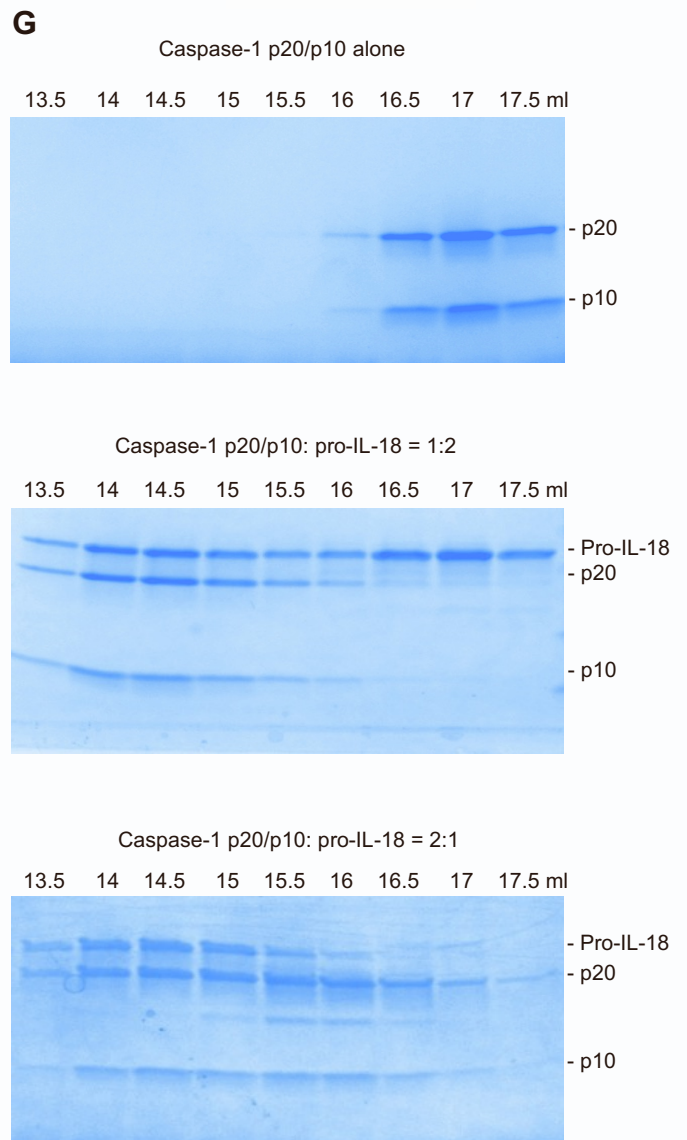
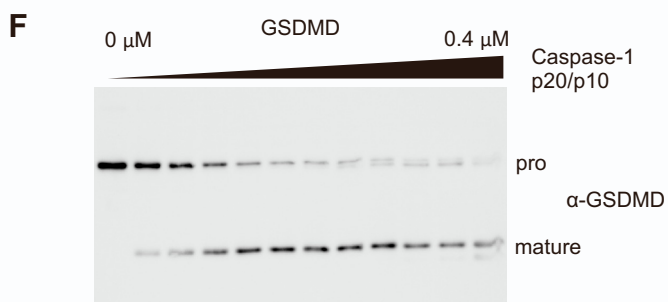
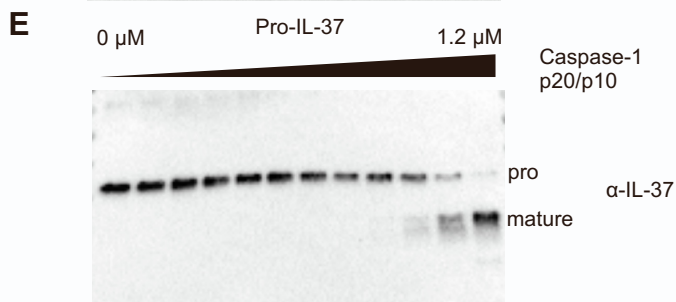
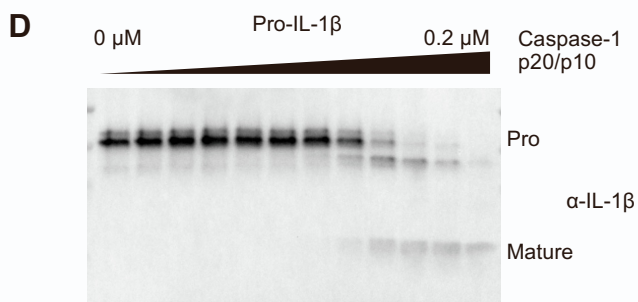
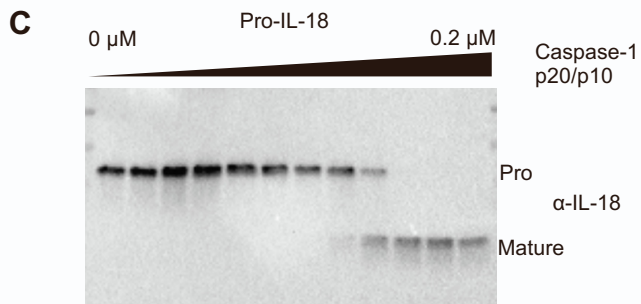
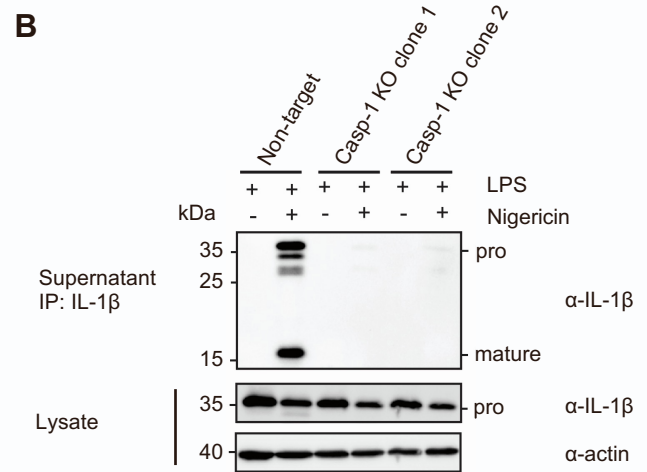
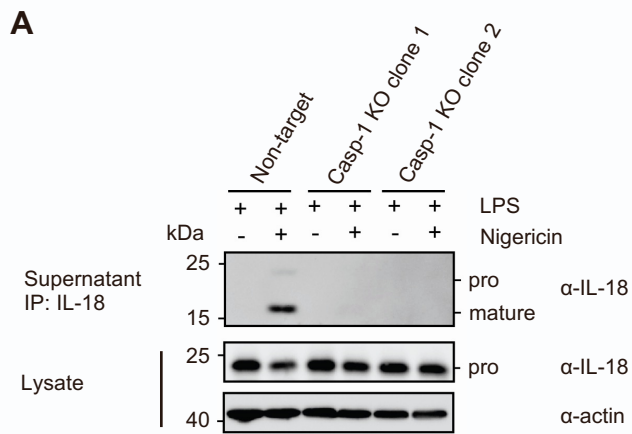


**Immunity, Volume 57**

## **Supplemental information**

### **Structural transitions enable interleukin-18 maturation and signaling**

**Ying Dong, Jeffrey P. Bonin, Pascal Devant, Zhuoyi Liang, Alexander I.M. Sever, Julian Mintseris, James M. Aramini, Gang Du, Stephen P. Gygi, Jonathan C. Kagan, Lewis E. Kay, and Hao Wu**



**Figure S1. Biochemical characterization for the processing of different substrates by human caspase-1, related to Figure 1**

(A,B) Immunoblots for the non-target control and two clones (shown as clones 1 and 2) of caspase-1 knockout (KO) THP-1 macrophages primed with LPS for 4 h before treatment with nigericin for 2-3 h. IL-18 (A) and IL-1 $\beta$  (B) were immunoprecipitated from cell culture supernatants and analyzed by immunoblot.

(C-F) Immunoblots showing *in vitro* catalytic efficiency of caspase-1 on pro-IL-18 (C), pro-IL-1 $\beta$  (D), pro-IL-37 (E) and GSDMD (F). The concentrations displayed are active caspase-1 concentrations determined by active site titration assay, and are 2-fold dilution series.

(G) The SDS-PAGE of gel filtration fractions of caspase-1 p20/p10 (C285A catalytic mutant) alone, caspase-1 p20/p10 (C285A catalytic mutant) and pro-IL-18 mixed at 1:2 or 2:1 molar ratios, indicating that pro-IL-18 can dimerize caspase-1 p20/p10 at a substoichiometric ratio. The elution volume of individual fractions from a Superdex 200 column are indicated.

The data shown are representative of at least three independent experiments.

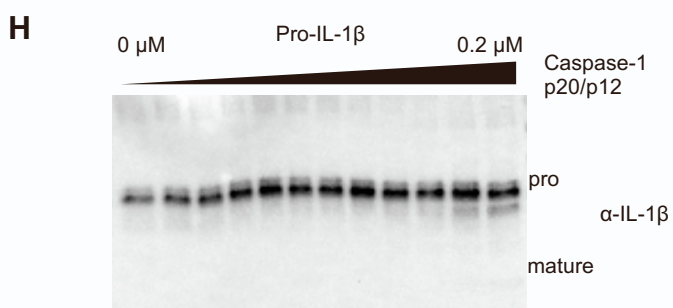
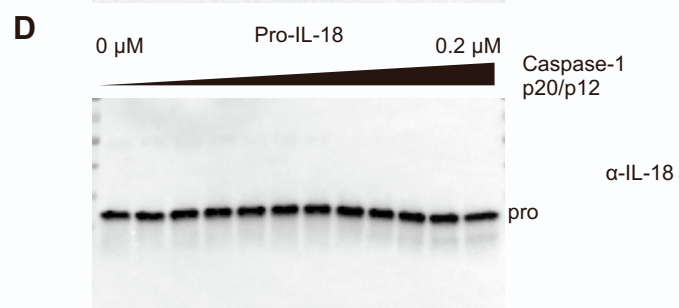
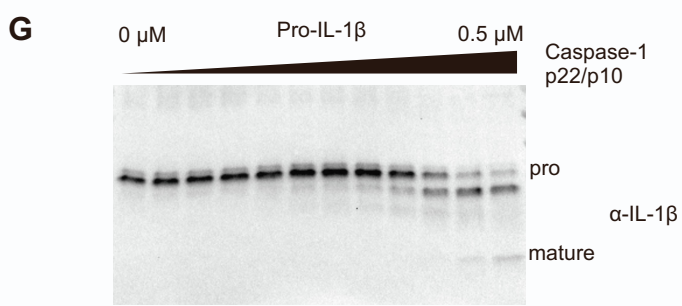
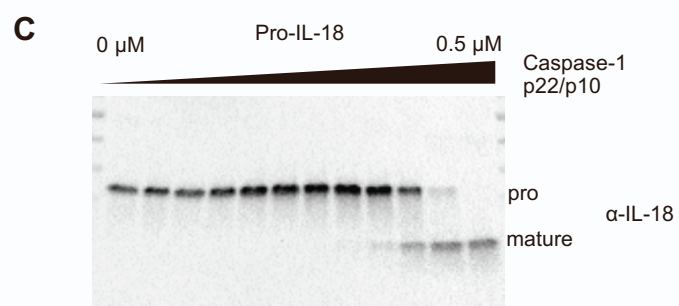
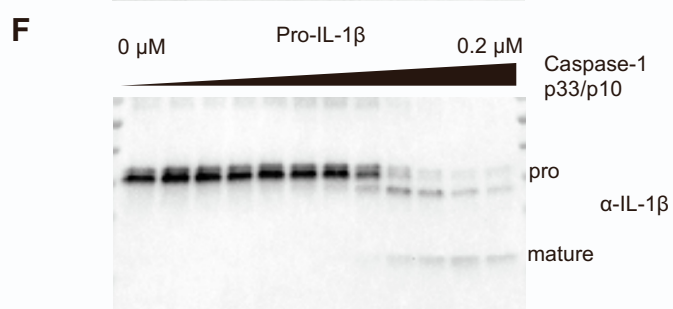
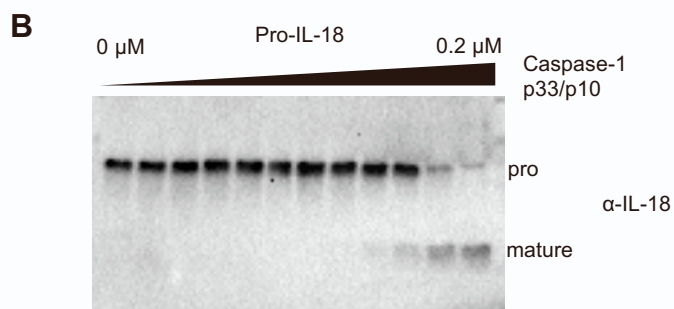
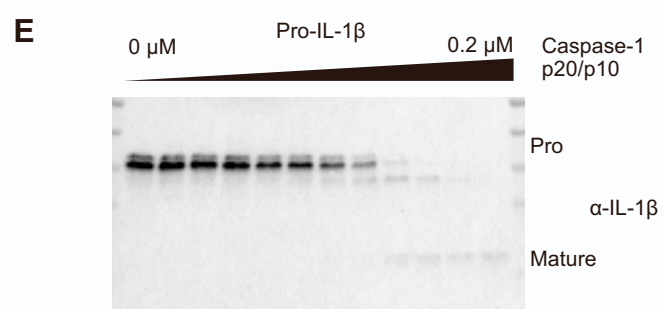
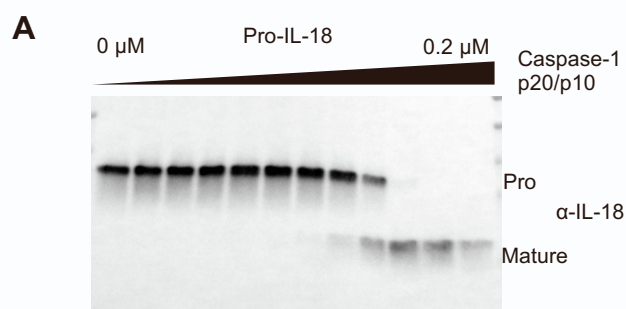
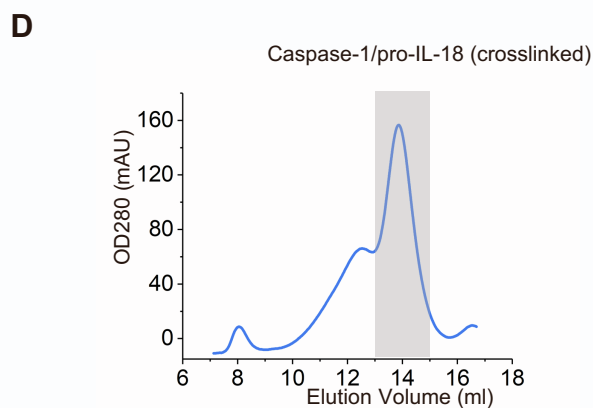
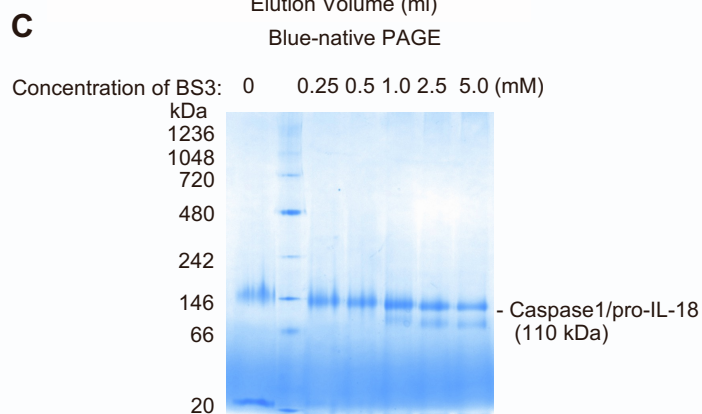
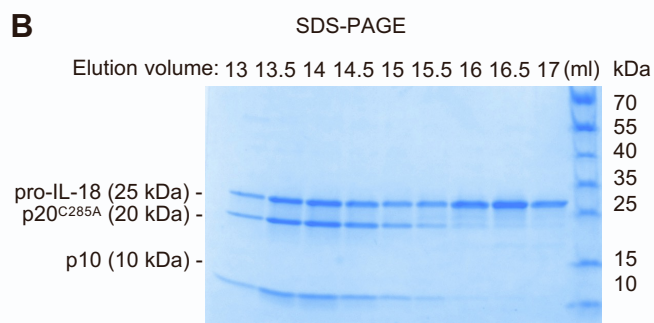
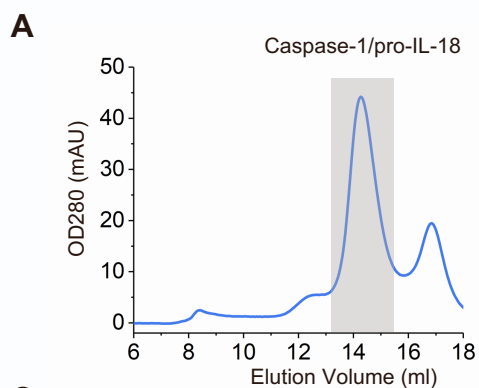




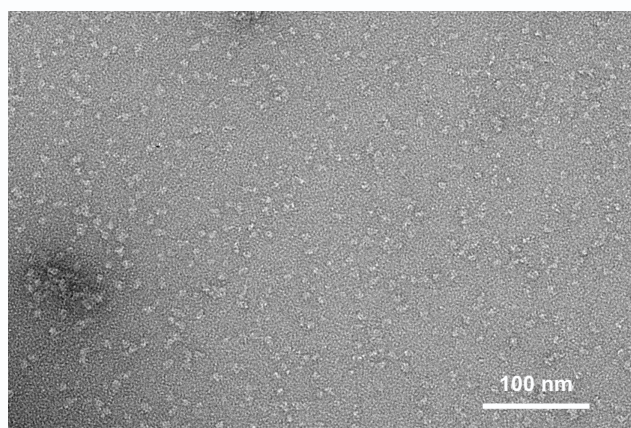
**Figure S2. Biochemical characterization for the processing of pro-IL-18 and pro-IL-1 $\beta$  by different auto-processed forms of human caspase-1, related to Figure 2**

(A-H) Immunoblots showing *in vitro* catalytic efficiency determination of indicated auto-processed forms of caspase-1 on pro-IL-18 (A-D) and pro-IL-1 $\beta$  (E-H). The concentrations displayed are active caspase-1 concentrations determined by active site titration assay, and are 2-fold dilution series. The data shown are representative of three independent experiments.



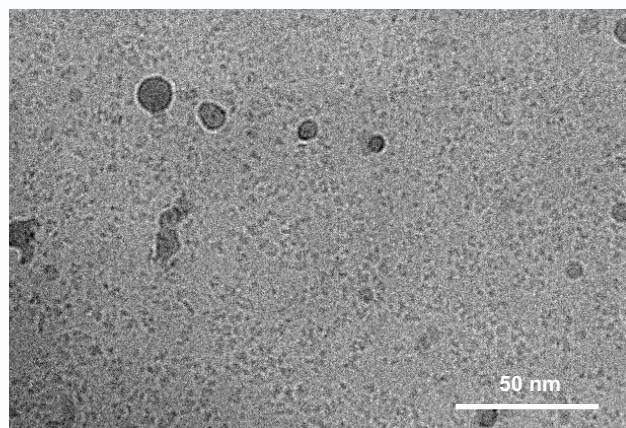
**E**

Negative staining raw image of caspase-1/pro-IL-18



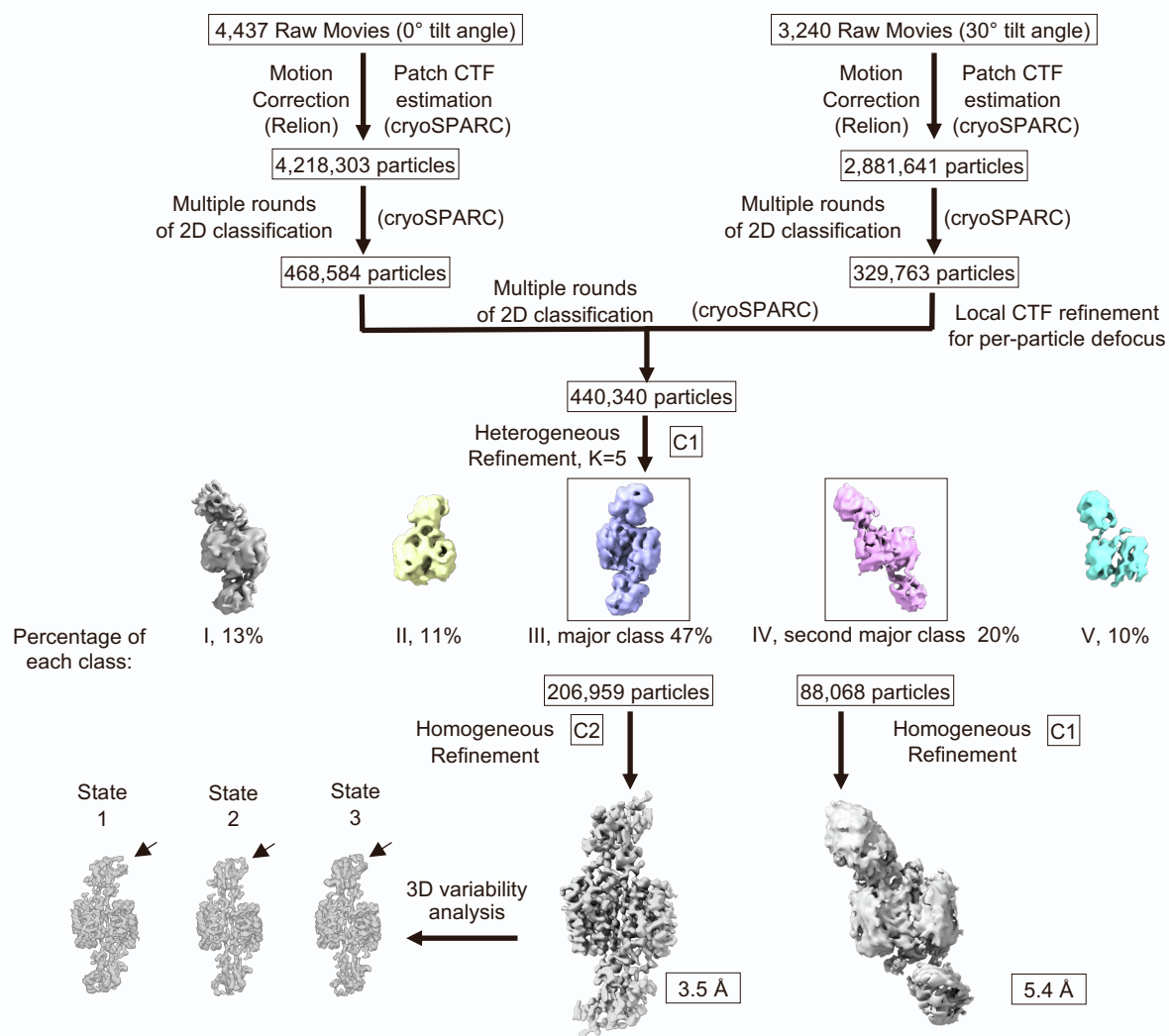
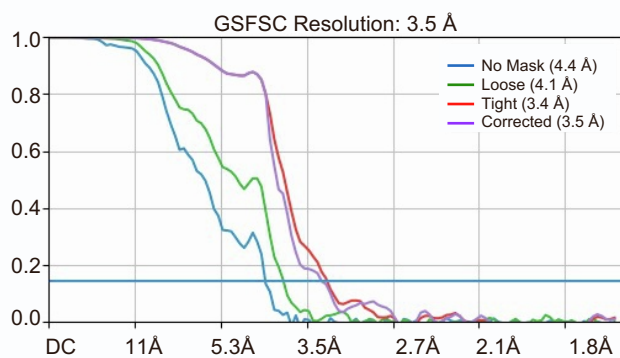
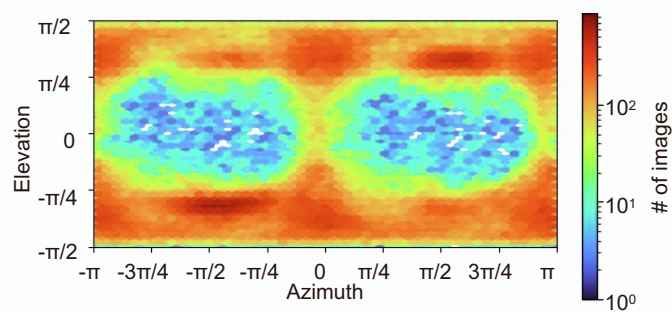
**F**

Cryo-EM raw image of caspase-1/pro-IL-18



**Figure S3. Preparation of the caspase-1/pro-IL-18 complex, related to Figure 3**

- (A) Gel filtration profile of the caspase-1/pro-IL-18 complex before crosslinking. The major peak collected for further biochemical analysis and cryo-EM sample preparation is indicated in the gray area.
- (B) SDS-PAGE gel of fractions from the gel filtration chromatography in (A).
- (C) Blue-native (BN) PAGE of the caspase-1/pro-IL-18 complex crosslinked by different concentrations of BS3 ranging from 0 - 5 mM.
- (D) Gel filtration profile of the caspase-1/pro-IL-18 complex from the peak in (A) crosslinked by 1 mM BS3.
- (E) Representative negative staining image of the caspase-1/pro-IL-18 complex.
- (F) Representative cryo-EM raw image of the caspase-1/pro-IL-18 complex.

**A****B****C****D**

Caspase-1/pro-IL-18 (color code consistent with Fig.3E-F) and Caspase-4/pro-IL-18 (color in gray) alignment at caspase region

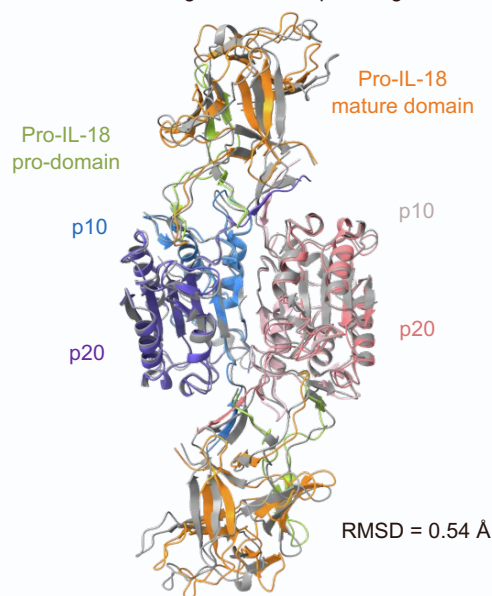


**Figure S4. Cryo-EM data processing for caspase-1 and pro-IL-18 complex, related to Figure 3**

(A) Cryo-EM data processing flow chart. The heterogeneous refinement results in five representative classes. The percentage of each class is shown. The major class and second major class are highlighted. The homogeneous refinement was performed with (C2) or without (C1) symmetry to obtain the final map for the two major classes. The 3D variability analysis was performed in CryoSPARC and showed three representative states from the major class. The flexible region of pro-IL-18 revealed by the 3D variability analysis is indicated by an arrow.

(B) Gold-standard FSC curves of the major class between two half maps, unmasked (blue), loosely masked (green), tightly masked (red), and corrected (purple).

(C) Angular distribution of the particles used for the final reconstruction of the major class.

(D) A superposition between the caspase-1/pro-IL-18 and the caspase-4/pro-IL-18 complexes. The caspase-1/pro-IL-18 complex (color code consistent with that in Fig. 3E-F) and the caspase-4/pro-IL-18 complex (PDB: 8SPB, in gray) are overlaid at the caspase region with a backbone heavy atom RMSD of 0.54. Pro-IL-18 molecules in the caspase-4 complex appear to be a bit more closed than those in the caspase-1 complex.

**A** Crosslinked lysine pairs between caspase-1 p10 and pro-IL-18

Caspase-1 p10	Pro-IL-18	Ca-Ca (Å)
317-AIKKA-321	40-KLESKLSVIRN-50	22.9
317-AIKKA-321	93-RGMAVTISVKCEKI-107	11.6
317-AIKKA-321	140-RSVPGHDNKMQFES SSYEGYFLACEKE-166	18.6
317-AIKKA-321	167-RDLFKLILKK-176	23.6
319-KKAHIEKD-326	17-KFIDNTLYFIAEDDENL ESDYFGKLESKL-45	19.8
319-KKAHIEKD-326	40-KLESKLSVIRN-50	16.1
319-KKAHIEKD-326	140-RSVPGHDNKMQFES SSYEGYFLACEKE-166	15.3

**C** Crosslinked lysine pairs between caspase-1 p20 and pro-IL-18

Caspase-1 p20	Pro-IL-18	Ca-Ca (Å)
246-KKHSEQVPDILQLNAI FNMLNTKNCPSLKD-275	140-RSVPGHDNKMQFES SSYEGYFLACEKE-166	12.9
259-RGDSPGVVWFKD-270	40-KLESKLSVIRN-50	22.2
259-RGDSPGVVWFKD-270	140-RSVPGHDNKMQFES SSYEGYFLACEKE-166	16.6
259-RGDSPGVVWFKD-270	167-RDLFKLILKK-176	18.0
259-RGDSPGVVWFKD-270	171-KLILKE-177	22.2

**E** Crosslinked lysine pairs within pro-IL-18, in caspase-1/pro-IL-18 complex

Pro-IL-18	Pro-IL-18	Ca-Ca (Å) in complex / IL-18
40-KLESKLSVIRN-50	148-KMQFESSSYEGYFLA CEKERD-168	18.7 / 33.6 Too far in IL-18
40-KLESKLSVIRN-50	171-KLILKE-177	13.8 / 31.9 Too far in IL-18

All the remaining pairs are consistent with structures of both the caspase-1/pro-IL-18 complex and mature IL-18 (PDB: 3WO2).

**G** One pro-IL-18 molecule binds

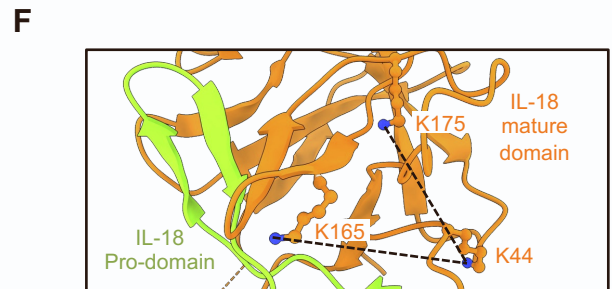
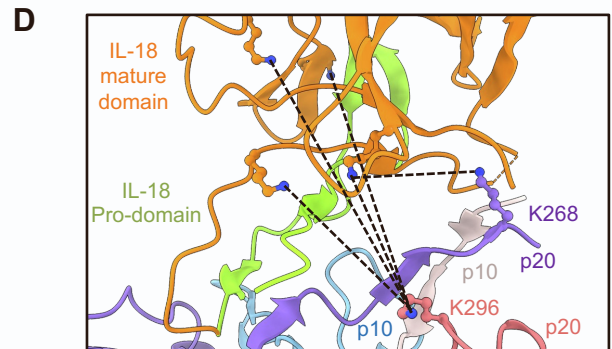
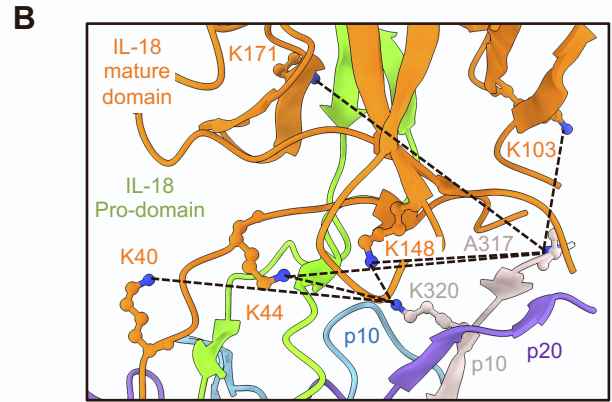
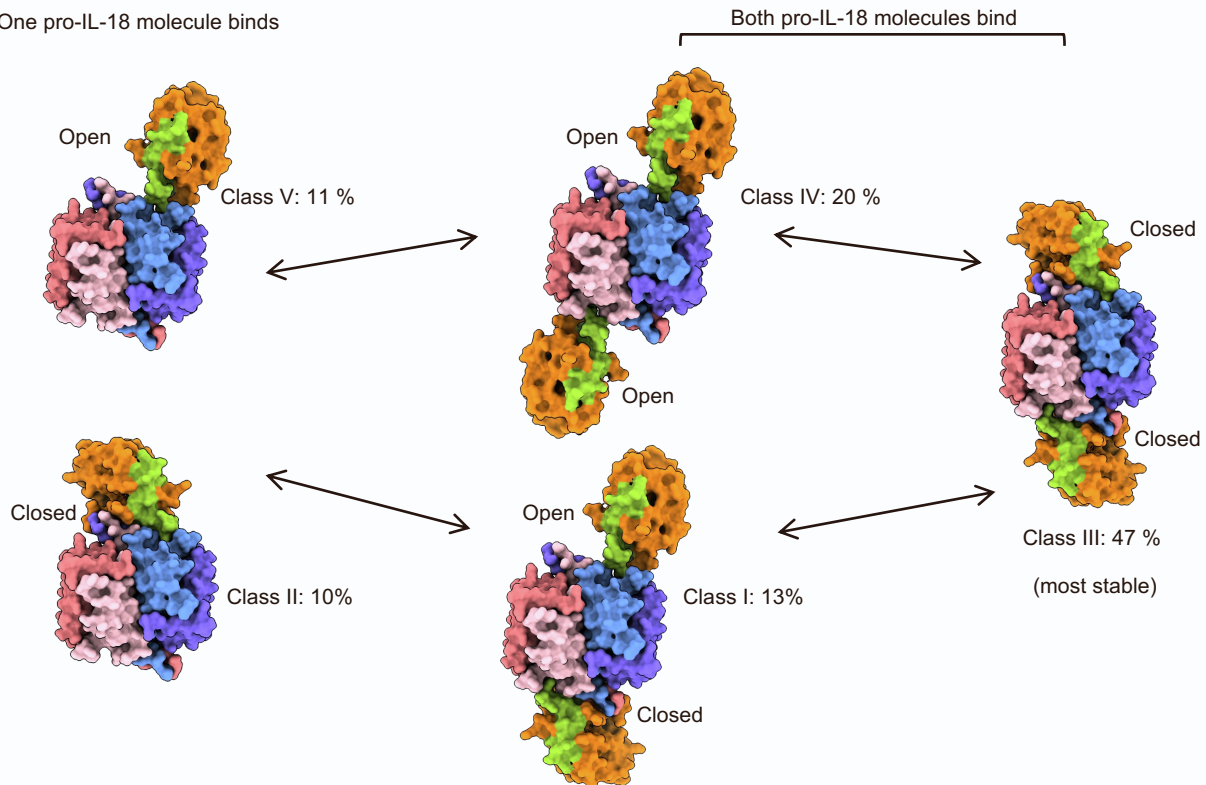




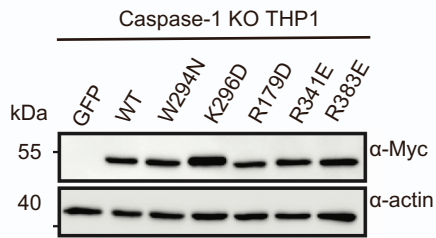
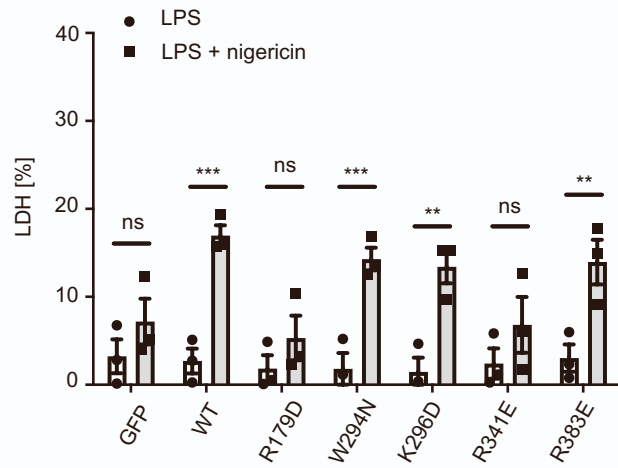
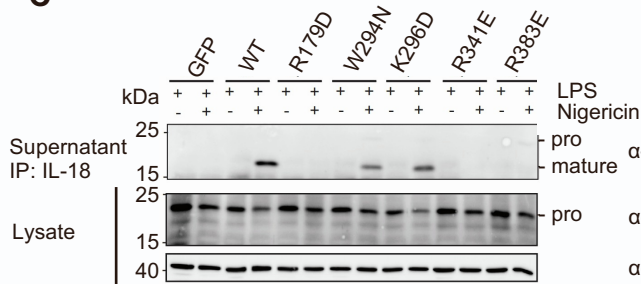
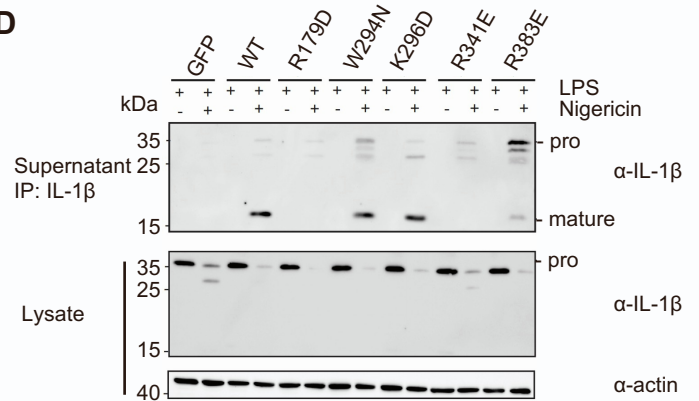
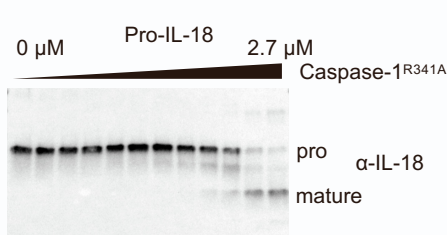
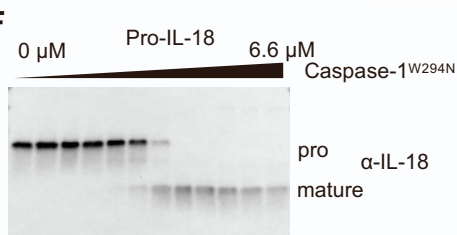
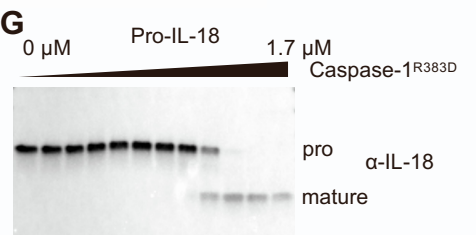
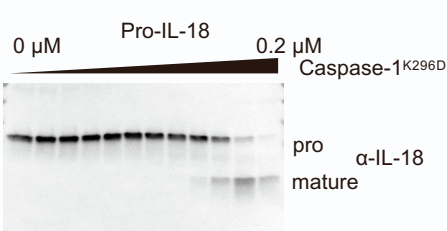
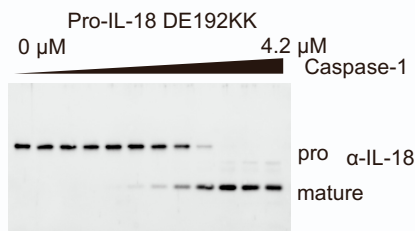
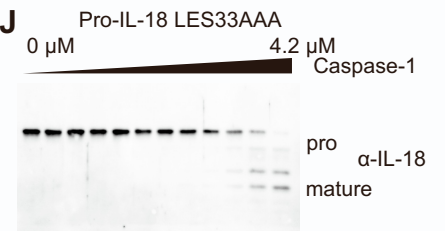
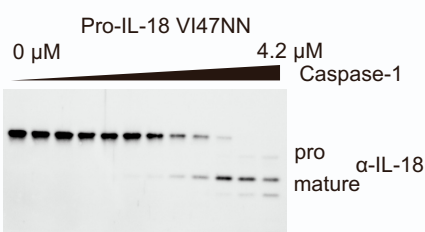
**Figure S5. Crosslinking mass spectrometry analysis of caspase-1/pro-IL-18, and variable modes of recognition of pro-IL-18 by caspase-1, related to Figure 3**

(A-B) Summary of BS3 crosslinked lysine pairs between caspase-1 p10 and pro-IL-18. The crosslinked peptides with high confidence are shown with residue ranges in their domain colors (A), and on the structure with black dotted lines (B).

(C-D) Summary of BS3 crosslinked lysine pairs between caspase-1 p20 and pro-IL-18. The crosslinked peptides with high confidence are shown with residue ranges in their domain colors (C), and on the structure with black dotted lines (D).

(E-F) Summary of BS3 crosslinked lysine pairs within pro-IL-18 in the caspase-1/pro-IL-18 complex. The crosslinked peptides with high confidence are shown with residue ranges in their domain colors (E), and on the structure with black dotted lines (F).

(G) Variable modes of recognition of pro-IL-18 by caspase-1 that involve only the active site or both the active site and the exosite. Presumably, both open and closed modes of interaction can result in pro-IL-18 processing by caspase-1.

**A****B****C****D****E****F****G****H****I****J****K**



**Figure S6. Mutations of key residues at the two interfaces impair the binding and cleavage of pro-IL-18 and pro-IL-1 $\beta$  by caspase-1, related to Figure 4 and 5**

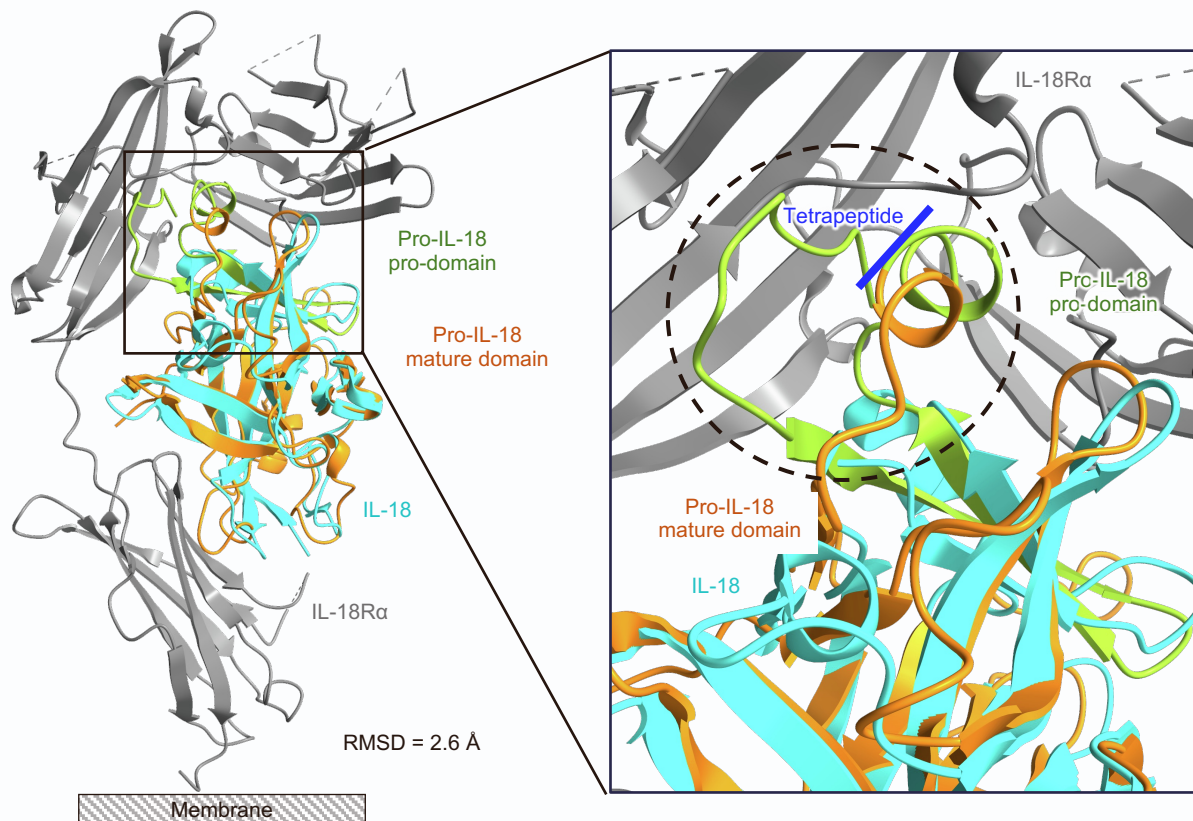
(A) Immunoblot showing stable expression of the indicated, Myc-tagged caspase-1 mutants in *CASP1*<sup>-/-</sup> THP-1 cells.

(B) LDH release from *CASP1*<sup>-/-</sup>KO THP-1 macrophages expressing indicated caspase-1 mutants primed with LPS for 4 h, or also followed by nigericin stimulation for 3 h.

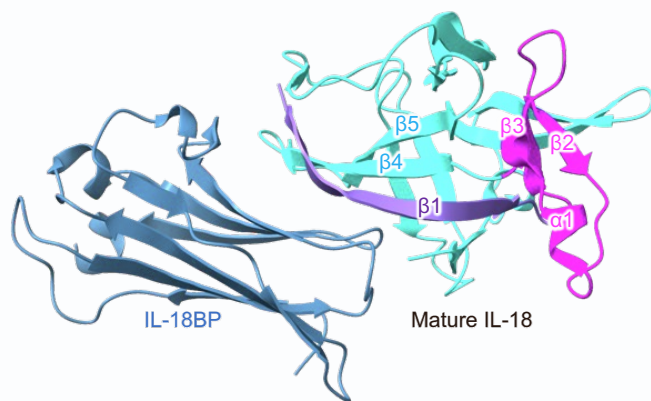
(C,D) Caspase-1-deficient THP-1 macrophages reconstituted with indicated caspase-1 mutants primed with LPS for 4 h before treatment with nigericin for 2-3 h. IL-18 (C) and IL-1 $\beta$  (D) were immunoprecipitated from cell culture supernatants and analyzed by immunoblot.

(E-K) Immunoblots showing *in vitro* cleavage of WT and mutant pro-IL-18 by WT and mutant caspase-1. Specific mutants used are indicated. The concentrations displayed are active caspase-1 concentrations determined by active site titration assay, and are 2-fold dilution series.

The data shown are representative of three independent experiments. Bars and error bars represent the mean  $\pm$  SEM of at three independent experiments. Statistical significance was determined by two-way ANOVA with Tukey's multiple comparisons test: \*\*p < 0.01; \*\*\*p < 0.001.

**A****B**

IL-18/IL-18BP complex (7AL7)



Pro-IL-18 superimposed with IL-18/IL-18BP complex (7AL7), pro-IL-18 is shown

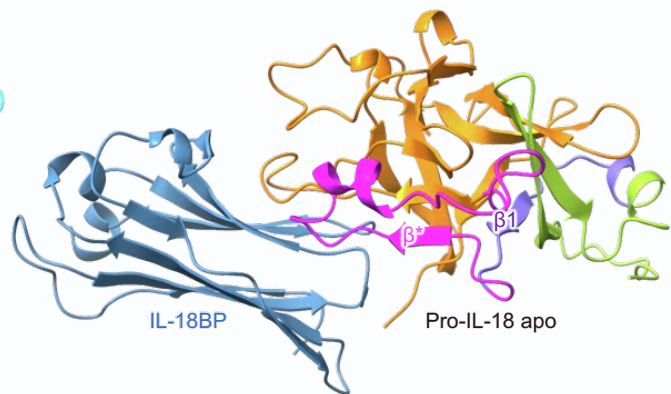


**Figure S7. Pro-IL-18 and mature IL-18 structures, related to Figure 7**

(A) Overlay of pro-IL-18 onto the IL-18/IL-18R $\alpha$  complex structure (PDB: 4R6U), showing the steric hindrance to receptor binding by the tetrapeptide motif region of pro-IL-18. The color code for the domains is consistent with that in Figure 7.

(B) The comparison of pro-IL-18 and mature IL-18 for IL-18BP binding. Pro-IL-18 apo is aligned with IL-18 in the IL-18/IL-18BP complex (7AL7). The  $\beta 2$ - $\beta 3$ - $\alpha 1$  region (magenta) in mature IL-18 rearranged from  $\beta^*$  and the following region in pro-IL-18 apo is not involved in the binding (left). The  $\beta^*$  and the following region in pro-IL-18 clash with IL-18BP binding. The short  $\beta 1$  in pro-IL-18 apo changes into the long  $\beta 1$  in mature IL-18 to mediate the interaction with IL-18BP. The color code for the domains is consistent with that in Figure 7.

**Table S1. Data Collection, processing and validation statistics, related to Figure 3**

<b>Data Collection and Processing</b>	
Microscope	Titan Krios
Voltage (keV)	300
Camera	K3
Magnification	105,000
Pixel size at detector (Å/pixel)	0.83
Total electron exposure (e <sup>-</sup> /Å <sup>2</sup> )	55.4
Exposure rate (e <sup>-</sup> /pixel/sec)	12.7
Number of frames collected during exposure	40
Defocus range (µm) (0° / 30° tilt angle)	-1.0 to -2.5 / -0.8 to -1.8
Automation software	SerialEM 3.8
Energy filter slit width (eV)	20
Micrographs collected (no.) (0° / 30° tilt angle)	4,437 / 3,240
Micrographs used (no.) (0° / 30° tilt angle)	4,377 / 2,459
Total extracted particles (no.) (0° / 30° tilt angle)	4,218,303 / 2,881,641
<b>Refinement</b>	
Refined particles (no.) / Final particles (no.)	440,340 / 206,959
Symmetry parameters	C2
Map resolution (Å)	3.5
FSC 0.143 (unmasked / masked)	3.5 / 4.4
Resolution range (Å)	3.2 to 8.8
Resolution range due to anisotropy (Å)	3.4 to 4.0
Map sharpening <i>B</i> factor range (Å <sup>2</sup> )	-165.1
Map sharpening methods	LocalDeblur
<b>Model composition</b>	
	6
Chains	792
Protein residues	
<b>Validation</b>	
Model-Map scores	
CC (correlation coefficients)	0.71
Average FSC (0 / 0.143 / 0.5)	2.7 / 3.5 / 4.2
R.m.s. deviations from ideal values	
Bond lengths (Å)	0.003
Bond angles (°)	0.755
MolProbity score	1.96
CaBLAM outliers	3.82
Clashscore	10.35
Poor rotamers (%)	0.7
C-beta outliers (%)	0.00
Ramachandran plot	
Favored (%)	93.43
Allowed (%)	6.19
Outliers (%)	0.39

**Table S2. Summary of NMR structural statistics for pro-IL-18<sup>a</sup>, related to Figure 6**

Parameters		
Completeness of resonance assignments <sup>b</sup>		
Backbone (%)		99.3
Side chain (%)		96.9
Aromatic (%)		97.8
Stereospecific methyl (%)		95.2
Conformationally-restricting restraints		
Distance restraints		
Total		4053
Intra-residue (i = j)		859
Sequential ( i-j  = 1)		1030
Medium range (1 <  i - j  < 5)		509
Long range ( i - j  ≥ 5)		1655
Dihedral angle restraints		
Total		136
φ + ψ		124
χ <sup>1</sup>		12
No. of restraints per residue		21.9
No. of long-range restraints per residue		8.7
Residual restraint violations <sup>c</sup>		
Average no. of distance violations per structure:		
0.1 - 0.2 Å		13.0
0.2 - 0.5 Å		11.1
> 0.5 Å		8.5
average RMS distance violation / constraint (Å)		0.34
Maximum distance violation (Å)		1.16
Average no. of dihedral angle violations per structure:		
1 - 10°		3.7
> 10°		0.1
average RMS dihedral angle violation / constraint (degree)		4.45
Maximum dihedral angle violation (°)		11.3
Model Quality		
RMSD backbone atoms (Å) <sup>d</sup>		0.50
RMSD heavy atoms (Å) <sup>d</sup>		0.73
RMSD deviation of bond lengths (Å)		0.010
RMSD deviation of bond angles (°)		0.3
No. of close contacts		4
MolProbity Ramachandran statistics <sup>d</sup>		
Most favored regions (%)		97.0
Additionally allowed regions (%)		2.9
Disallowed regions (%)		0.2
Global quality scores	Raw score	Z-score
Procheck (phi-psi) <sup>d</sup>	-0.32	-0.94
Procheck (all) <sup>d</sup>	-0.09	-0.53
MolProbity clash score	8.51	0.07

<sup>a</sup> Structural statistics were computed using PSVS 2.0<sup>60</sup> and PDBStat 5.23.08.<sup>59</sup>

<sup>b</sup> Calculated from the total expected number of peaks excluding highly exchangeable protons (N-terminal, Lys, and Arg amino groups, hydroxyls of Ser, Thr, and Tyr, free thiols of Cys, carboxyls of Asp and Glu, and non-protonated aromatic carbons).

<sup>c</sup> Average distance violations were calculated using sum over  $r^6$ .

<sup>d</sup> Calculated for ordered residue ranges based on <sup>15</sup>N relaxation data: 11-28,45-60,80-88,97-104,107-112,114-120,133-145,147-165,170-179,185-190.